Mapping *Ae. aegypti* Bird Bath Habitats for Implementing "Seek and Destroy" Larval Source Management in Hillsborough County, FL. USA

Kristen Keana Ritchie[1, *], Ricardo Lzurieta[2], Ismael Hoare[2], Namit Choudhari[3], Kayleigh Murray[2], Brooke Yost[4], David Fiess[5], Paolo Pecora[5], Anthony Masys[2], Jesse Casanova[2], Benjamin George Jacob[2]

[1]Department of Global Communicable Diseases, College of Public Health, University of South Florida, Tampa, USA

[2]Department of Global Health, College of Public Health, University of South Florida, Tampa, USA

[3]School of Geosciences, University of South Florida, Tampa, USA

[4]Department of Epidemiology, College of Public Health, University of South Florida, Tampa, USA

[5]Hillsborough County Abatement Office, Tampa, USA

Email address:

kristenr2@usf.edu (Kristen Keana Ritchie), ricardoi@usf.edu (Ricardo Lzurieta), ihoare@usf.edu (Ismael Hoare), nchoudhari@usf.edu (Namit Choudhari), kmurray10@usf.edu (Kayleigh Murray), byost1@usf.edu (Brooke Yost), fiessd@HCFLGov.net (David Fiess), pecorap@HCFLGov.net (Paolo Pecora), tmasys@usf.edu (Anthony Masys), jcasanov@usf.edu (Jesse Casanova), mbjacob1@usf.edu (Benjamin George Jacob)

[*]Corresponding author

Abstract: Bird baths pose a threat to human life as they are the perfect foci for Aedes aegypti Linnaeus, a mosquito that can spread chikungunya, Zika fever, Rift Valley fever, Mayaro, Yellow fever, and dengue under the right temperature and precipitation conditions. The vector lays its eggs in containers with standing water, which later emerge as blood-feeding adult females that can transmit these viruses. Unfortunately, past entomological models contributed to literature have not been able to predictively map precise geolocations of aquatic larval habitats of Ae. aegypti. This is primarily due to limited remote sensing tools [e.g., acquiring epi-entomologic habitat data using ground-level survey with a Google Map, differentially collected Global Positioning Systems (GPS) tracker, etc.]. Thus, many Ae. aegypti habitats may go undetected even in open, canopied, land cover areas. We employed ArcGIS Pro, Python, and R to develop multiple satellite spectral signature models for predicting Ae. aegypti bird bath habitats in Hillsborough County, Florida. We interpolated a georeferenced, county abatement, high-income, residential, bird bath, Red, Green, and Blue [RGB], Sentinel-2, 10-meter resolution, spectral signature in Python. Incorporating other prolific, Ae. aegypti, larval/pupal habitat, seasonal, gridded, zip code, land use/land cover [LULC], stratified, Normalized Difference Vegetation [NDVI], and elevation satellite maps allowed eco-cartographically distinguishing unknown potential super breeder foci backyards [> 3 bird bath larval/pupal habitats] as well as individual aquatic breeding site foci in the intervention, county abatement, study site. Since we knew the aquatic habitat data occurrence abundance and distribution, a priori, eigen-autocorrelation, eigen-spatial filter algorithm attempted to spatially geolocate potentially hyperendemic clustered habitat patterns [i.e., 'hot spots'] and dispersed habitat patterns [i.e., 'cold spots']. We subsequently field-verified the habitat signature entomological habitat model forecasts. The sensitivity and specificity of the ground truth exercises revealed a model approaching 100 percent for identifying aquatic, birdbath, Ae. aegypti, larval habitats. The Moran's Index [I] indicated slight geospatial negative autocorrelation; [Moran's Index: -0.143071, z-score: -1.057957, p-value: 0.290075], hence the breeding site aquatic foci were dispersed. Remote sensing data can be used for constructing LULC, NDVI, elevation and signature models which can be used for implementing "Seek and Destroy" a real-time larval source management [LSM] system for informing individual homeowners and residents using social media for removing standing water in bird baths, twice a week.

Keywords: *Ae. aegypti*, Bird Baths, Signature, Python, Seek And Destroy, Hillsborough County, Fl

1. Introduction

Marked geographic, spatiotemporal (henceforth, geospatiotemporal) variabilities in mosquito infection of arboviruses require adaptive strategies for determining optimal field-sampling timeframes, pool screening, and data analyses. In particular, the error distribution and aggregation patterns of adult arboviral mosquitoes can vary significantly by species, which can statistically bias analyses of geospatiotemporal geosampled signature predictor variables generating misinterpretation of prolific habitat surveillance geolocations. Currently, there is a lack of reliable and consistent measures of risk exposure based on fieldgeosampled georeferenced explanatory signature-related, reflectance habitat, wavelength satellite covariates which can compromise quantitative predictions generated from arboviral mosquito surveillance models for implementing larval source management (LSM) strategies targeting hyperproductive, seasonal habitats. In this experiment, we employed spatial statistics and Sentinel-2 visible and nearinfra-red [NIR] data for determining trapping sites that were related to bird bath habitats of *Ae. aegypti* species and distribution in Hillsborough County Florida. Initially, a Land Use Land Cover (LULC), normalized difference vegetation index [NDVI], normalized difference water index [NDWI] and 3DEM models were constructed from multiple geospatiotemporal, geosampled, georeferenced signature, habitat predictors and the Sentinel-2 visible and NIR data. A Google Earth habitat model was also constructed. We then eigendecomposed the data into positive and negative eigenspatial filter eigenvectors. Eigendecomposition of *Ae. aegypti* habitats necessitates synthesizing orthogonal meteorological, land cover vegetation, elevation, and habitat variables in eigenvector eigen-geospace [13]. An autoregressive process in the error term was subsequently employed used to derive the sample distribution of the Moran's statistic for determining latent geo-spatial temporal eigen-autocorrelation components in the model. A Moran's index of spatial autocorrelation, involves the computation of cross-products of mean-adjusted values that are geographic neighbors (i.e., covariations), that ranges from roughly -1, to 0 to for negative, and nearly 0 to approximately 1 for positive, spatial autocorrelation, with an expected value of $-1/(n-1)$ for zero spatial autocorrelation, where n denotes the number of areal units [10]. Spatial autocorrelation has many interprets: a nuisance parameter, self-correlation, map pattern, a diagnostic tool, a missing variables surrogate, redundant information, a spatial process mechanism, a spatial spillover, and the outcome of areal unit demarcation [10]. Eigen-spatial filter algorithms established means, variances, distributional functions, and pairwise correlations for the Sentinel-2 signature, habitat prognosticative variables. In doing so, we assumed that the eigenfunction spatial filter would quantify the residual autocorrelation error in the mean response term of the model as a linear combination of various distinct aquatic signature-related, *Ae. aegypti* bird bath habitat map patterns. Our assumption was seasonally prolific bird bath habitats of *Ae. aegypti* can be accurately geospatiotemporally targeted based on signature georeferencable data using Sentinel-2 satellite signature model topographic geomorphological explanatory covariates, and space–time eigenfunctions.

Florida's subtropical climate is the ideal destination for tourists and the 84 different species of mosquitos who have made this state their home. A particular species of mosquito, the *Ae. aegypti*, is the vector for many mosquito-borne illnesses such as dengue, Zika virus, yellow fever, and West Nile virus, all of which have become endemic diseases in the state. Due to historical records of yellow fever and dengue, *Ae. aegypti* has been thought to be present in Florida as early as the seventeenth century [5]. This highly invasive mosquito is typically found in areas of human-populated environments, which makes Hillsborough County, FL, an ideal location to take blood meals and to breed. Human blood meals give the female mosquitos the nutrition they need during their gonotrophic cycle (reproductive cycle) to develop their eggs. The duration of an *Ae. aegypti*'s gonotrophic typically lasts 3 to 4 days and can determine the rate at which the female mosquito will take a blood meal [1, 24, 34]. It is to be noted that there is a difference between biting and taking a blood meal. When a mosquito bites (also known as probing), the mosquito will use a sensory probe called the labella to search for blood vessels through the skin. Once a mosquito senses a blood vessel, it will use its fascicle to penetrate and release saliva that can transfer a pathogen to the human [1]. Once the mosquito's fascicle lacerates a blood vessel, its stylet begins the blood-feeding process [1, 7, 24]. Whether or not the bite results in a blood meal, it places the human at risk if the mosquito's saliva contains an infectious agent (i.e., dengue).

Focal outbreaks of dengue fever (dengue) in the state of Florida have increased since 2009 (Stephenson et al. 2021). There have been ten locally acquired cases in Florida this year. Four new cases of the locally acquired mosquito-borne illness dengue fever alone were reported in Broward and Miami-Dade counties between July 30 and August 5, 2023 [https://www.floridahealth.gov/]. However, little is known about the precise geolocations of *Ae. aegypti* habitat populations across different regions of Florida at the county level.

The *Ae. aegypti* species of mosquito is widely distributed throughout the state, occupying both artificial and natural containers [8, 12, 13, 29]. As of 2016, numerous abatement programs within the state conducted their own unique routine mosquito control surveillance, but unfortunately, Florida lacks a statewide, centralized reporting system where counties can share collected data [18]. With *Ae. aegypti* being strongly associated with highly populated urban areas, there is reason to believe that the risk of arbovirus within Florida's urban

areas is rising.

Many Floridian counties' efforts to reduce mosquito populations rely on trapping techniques or insecticides that target adult mosquitoes in their respective habitats [27]. While controlling the adult population of mosquitoes has been pivotal in reducing infected adults, the efficacy of the insecticide is questionable. Many mosquito populations, especially *Ae. aegpyti* can adapt to having resistance to both adulticides from the pyrethroid and organophosphate chemical classes [2, 19, 21, 22]. From a public health perspective, it is imperative that control methods target the immature stage of the mosquito's life cycle to reduce the growth of their populations and reduce the risk of mosquitoborne diseases.

Advances in computer vision have made it possible to get credible intelligence from satellite imagery using AI techniques such as Deep Learning in ArcGIS Pro. For example, ArcGIS Pro allows the usage of machine learning classification [e.g., Random Forest (RF)] object-based algorithmic methods for georeferenceable, satellite imaging, vector arthropod, seasonal, archived, remotely sensed, RGB, drone acquired, signature data [14]. Random Forest ensemble models are made of many decision trees using bootstrapping, random subsets of features, and average voting to make predictions [17]. Here, the improved ability of multispectral sensors and the statistical and machine learning computational geoprocessing tools in ArcGIS Pro provided real-time, sensing data resource for heuristically optimizing spatial data visualization of retrievable, seasonal, quantitative, thematic information [e.g., Sentinel-2 imaged, high income, urban residential land cover of a georeferenced, semipermanent, capture point, *Ae. aegypti* bird bath, aquatic, larval habitat] in a real-time geospatial AI, web configurable interactive database. Subsequently, we scaled up the RGB indexed spectral signature database of the Sentinel-2, imaged, capture point, zip code grid-stratified, LULC classifiable, scalable, habitat feature attributes [e.g., levels of canopy vegetation, 3-D slope coefficients of catchment watersheds, etc.] using geo-AI intelligence for predictively mapping unknown, georeferencable, county level, larval, aquatic bird bath, *Ae. aegypti* breeding sites for implementing real-time LSM "Seek and Destroy" (S&D).

Jacob et al. provide essential insights into implementing a new, real-time LSM for reducing larval, vector density [Macro S&D] and blood parasite level [Micro S&D] in a treated and suspected intervened malaria mosquito *Anopheles* [*gambiae* s.l., *arabiensis* s.s., *funestus* s.s.] habitat population which may be usable for treating *Ae. aegypti* bird bath habitats in Hillsborough County [14]. Initially, the authors of Jacob et al. constructed a geo-AI, iOS interactive, webconfigurable smartphone app for precisely ecogeographically geolocating georeferencable water bodies, including natural water bodies, irrigated rice paddies, cultivated swamps, ditches, agricultural ponds, and other geolocations, which are among the common breeding sites for *Anopheles* mosquitoes in Gulu district of Northern Uganda [14]. Satellite signature interpolation modeling may allow determining exact geolocations of

unknown *Ae. aegypti* habitats in a county or district for implementing S&D.

We hypothesized by integrating real-time, scaled-up spectral signature with satellite high-resolution data using geo-AI infused into an iOS application (app), a local vector control officer could retrieve a ranked list of visually similar breeding sites, aquatic foci of *Ae. aegypti* mosquitoes, and their respective, scalable, county-level, capture point, GPS indexable, habitat, and centroid coordinates. In this experiment, Spatial satellite signature models were extended to account for any non-Gaussian, *Ae. aegypti* geo-sampled, habitat count variables. Geospatial outliers were teased out in the residual plots. Subsequently, the *Ae. aegypti* habitat data were eco-epidemiologically signature forecasted. The model data included LULC, NDVI, and meteorologically derived, probabilistic, discrete, integer values which then were employed to prognosticate a number of habitat occurrences for the Hillsborough County study site. Jacob et al. confirmed that a signature land cover, vegetation, and 3D slope coefficients for a spatial autoregressive forecast model revealed geolocations of *Ae aegypti* habitat such as small containers, vases, flowerpot dishes, and tree holes [13].

Controlling populations of vector mosquito species in urban environments is a major challenge. *Ae. aegypti* is well adapted to and will successfully exploit many artificial and natural habitats present in urban environments, presenting a major challenge for the development of control strategies [31]. Reactive control strategies based on the use of larvicide and adulticide are widely ineffective due to the inherent difficulty in reaching cryptic breeding habitats and resting adult mosquitoes [23]. Moreover, *Ae. aegypti* populations have high levels of insecticide resistance which will further impair the effectiveness of reactive mosquito control strategies in urban environments [16].

Alternative vector control strategies such as S&D and their effectiveness in controlling not only *Aedes* mosquito populations but also in decreasing the incidence of arbovirus transmission are yet to be proven. Controlling populations of vector mosquitoes in urban and non-urban areas is a difficult task and control strategies based on the LSM framework are complex relying on many actions that rationally build on each other [25]. However, the key components of S&D such as mosquito surveillance, source reduction (i.e., aquatic habitat removal), community engagement, and improved policies can achieve great success. Therefore, being able to determine the role of the aquatic habitats that are widely present in urban and nonurban elevated and vegetated LULC, classified signature areas responsible for maintaining *Ae. aegypti* populations will allow not only the development of more effective preventative mosquito control strategies but would also help guide and improve policy and better inform the Hillsborough community. Our objectives in this article were: 1. To construct a Google Earth map of a georeferenced *Ae. aegypti* bird bath, capture point. 2. to extract a satellite signature of the aquatic breeding site foci: and, 3. To autocorrelate and interpolate the signature to find unsampled, unknown birdbath habitat and scalable, capture point, aggregated/non-aggregated, ['hot' and 'cold'

spot] countylevel geolocations for implementing S&D LSM control tactics in Hillsborough County, Florida.

2. Data Source and Methodology

2.1. Study Site

Hillsborough County is located in the west-central portion of the US state of Florida. In the 2020 census, the population was 1,459,762, making it the fourth-most populous county in Florida and the most populous county outside the Miami metropolitan area. A 2021 estimate has the population of Hillsborough County at 1,512,070 people with a yearly growth rate of 1.34%, which itself is greater than the populations of 12 states according to their 2019 population estimates. Its county seat and largest city is Tampa.

Hillsborough County is part of the Tampa–St. Petersburg–Clearwater Metropolitan Statistical Area. According to the US Census Bureau, the county has a total area of 1,266 square miles (3,280 km^2), of which 1,020 square miles (2,600 km^2) are land and 246 square miles (640 km^2) (19.4%) are covered by water. About 158.27 miles (254.71 km) of shoreline are on Tampa Bay. [www.wikipedia.org]
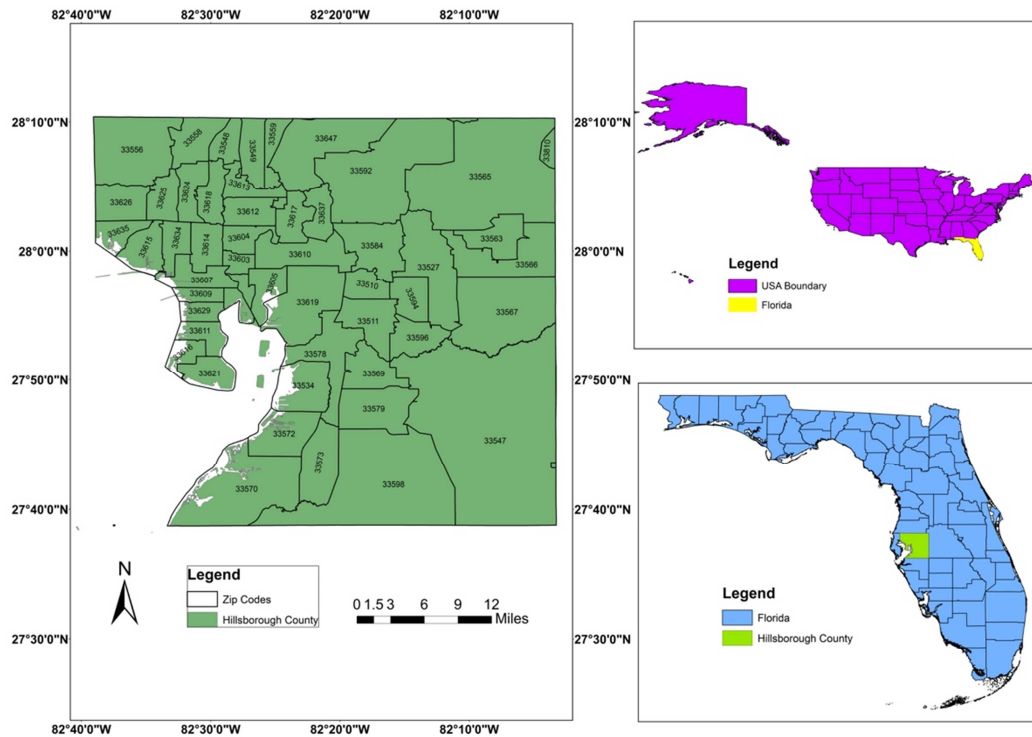

Figure 1. Study area map of Hillsborough County, FL.

2.2. Data Source

The European Space Agency's (ESA) high-resolution cloud-free, orthorectified, radiometric, and atmospherically corrected Sentinel 2B MSI (Multispectral Instrument) Level1C image of May 2023 was used for signature determination.

The satellite image was obtained from ESA's Copernicus Open Access Hub
(https://scihub.copernicus.eu/dhus/#/home). MSI sensors are widely used in mapping and monitoring LULC patterns, including farmlands, water bodies, and vegetation [15]. Each tile of Sentinel 2B Level-1C data covers 100×100 km^2, which is orthorectified in UTM/WGS84 projection [9]. Highresolution USGS 1/3 arc-second Digital Elevation Model (DEM) dataset of 10-meter spatial resolution from the National Elevation Dataset (NED) was downloaded from the Open   Topography (https://portal.opentopography.org/raster?opentopoID=OTNE

D.012021.4269.1) to identify sinks and generate the slope, stream order, and flood vulnerability map.

2.3. Land Use/Land Cover (LULC)

High-level thematic resolution land cover classes were mapped using supervised classification in Google Earth Pro for 2023 and 2022. Based on the existing knowledge of the study area's land use/land cover, five LULC categories were classified, viz., urban commercial, urban residential, rural, farmlands, and vegetation, to analyze the impacts of various LULC patterns and the potential *Ae. aegypti* bird bath habitats. Supervised classification has been extensively used for mapping land use/land cover classes [6]. Google Earth Pro provides accessibility to a high-resolution satellite image of less than 5 meters [6] compared to the Sentinel 10-meter resolution. This high-resolution satellite image avoids overlapping or misclassifying pixels in the other land cover classes, eliminating the noise and increasing a model's accuracy [6]. Moreover, the land use classes with the finer

thematic resolution, such as urban commercial and urban residential, and their difficulties in differentiating the spectral signatures that are residential, and their economic impacts cannot be captured using Landsat or Sentinel imagery alone due to the difficulties in differentiating the spectral signatures that are homogenous with other land use and land covers.

Verification points were randomly generated in ArcGIS Pro.

MLC gave the projected class values for the verification points. An error confusion matrix was not generated. The capture points were overlayed onto *Ae. aegypti* bird bath habitat hotspots of Uelmen et al., which revealed that the projected points generated from the MLC aligned exactly with our verification points [27].
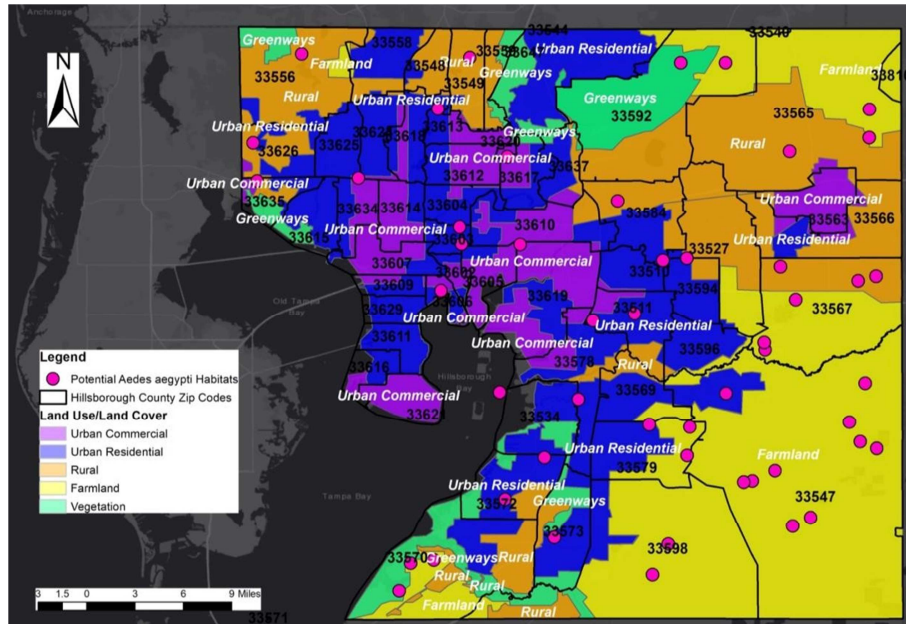

Figure 2. Zip code stratified land cover map of Hillsborough County, FL.

2.4. Normalized Difference Vegetation Index (NDVI).

NDVI is one of the most widely used remote sensing index [28], which explains the difference between visible (red band) and near-infrared [26]. The red band has a wavelength of 0.66 μm, and a near-infrared (NIR) band has 0.86 μm. The value of NDVI ranges from positive to negative. Positive values indicate dense vegetation areas; zero or negative values represent sparse vegetation or water/built-up areas. The formula for NDVI is given by Tucker (1979) as.
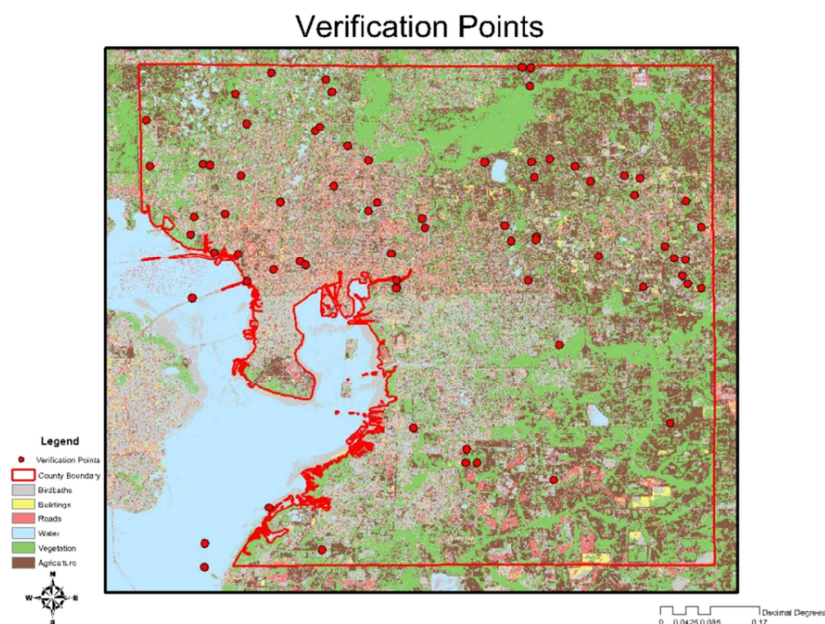

Figure 3. Verification Points.

$$\text{NDVI} = \frac{NIR - Red}{NIR + Red}$$

The NDVI values were subsequently retrieved at each geospatially geolocated potential, capture point sentinel site aquatic *Ae. aegypti* habitat to evaluate the association between these habitats and changes in vegetation as their habitats are found in areas with high vegetation and woodland [4, 13]. Thus, we hypothesized that the potential aquatic habitats of *Ae. aegypti* are generally found in areas of dense vegetation with high woods.
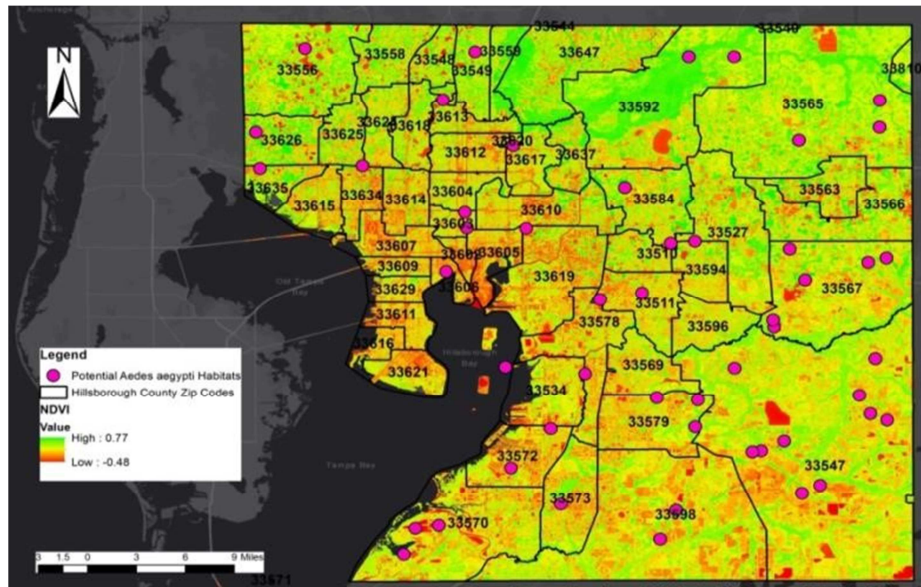

Figure 4. Zip code stratified normalized difference vegetation index of Hillsborough County, FL.

2.5. Digital Elevation Model (DEM)

High-resolution Digital Elevation Model (DEM) of ALOS PALSAR DEM data of 12.5-meter spatial resolution (Scene 1:Path-152, Frame-550; Scene 2: Path-152, Frame-540; acquisition date of the DEMs: April 26, 2010) was downloaded from the Alaska Satellite Facility [Earthdata Search | Earthdata Search (nasa.gov)]. The values of elevation were later extracted at each geospatially located potentially interpolatable *Ae. aegypti* birdbath habitat to analyze the relationship between these habitats and changes in elevation as they are generally found in areas of low elevation, especially in dense vegetation and in swamps or marshy lands [13]. Thus, we hypothesized that the potential habitats of *Ae. aegypti* are found in areas of low elevation, dense vegetation, and high woodlands.
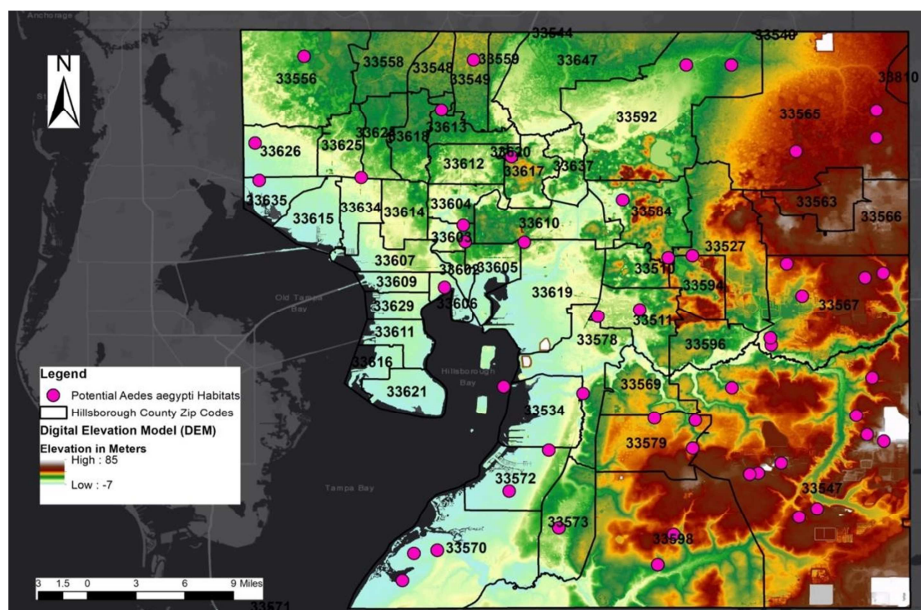

Figure 5. Zip code stratified digital elevation model of Hillsborough County, FL.

2.6. Autocorrelation Analyses

The first step for constructing a robust, georeferenceable, eigenizable, mosquito vector, arthropod, prognosticative, and epidemiologic risk model in R, is to specify the model [14]. Suppose an estimated, semi-parametric, geo-spatiotemporal, eigen-autocorrelation, aggregation/non-aggregation-oriented, georeferenceable, determinant vector arthropod vulnerabilityoriented model is misspecified. In that case, it will be biased and inconsistent [14]. In operationalizable, geospatiotemporal, regression-based, vulnerability-oriented, epidemiologic, *Ae. aegypti*-related, prognosticative, larval habitat models, the term misspecification covers a broad range of modeling errors, including measurement errors and discretizing, geo-sampled, continuous, prognosticative variables [8].
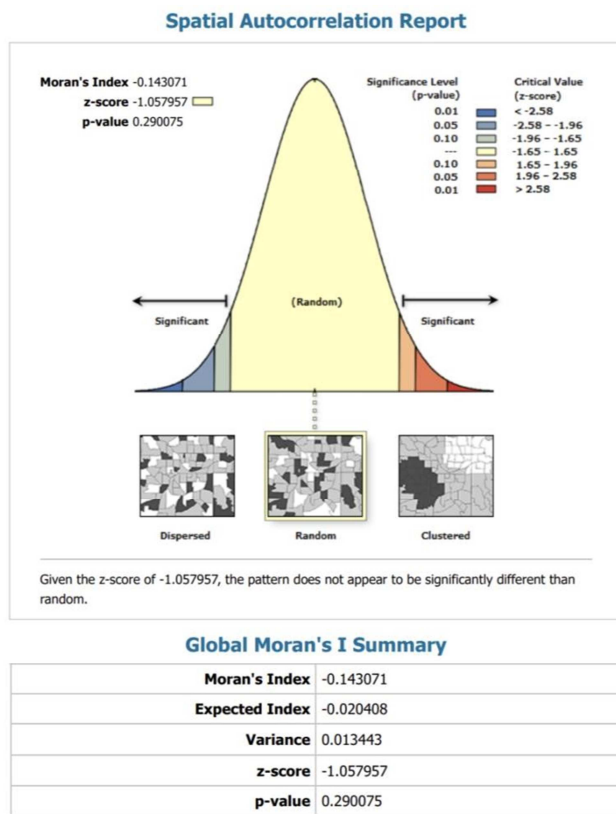

Figure 6. *Moran's index describes the distribution of Aedes aegypti bird bath habitats in Hillsborough County, FL.*

We generated spatial eigen-autocorrelation indices employing the capture point, georeferenced *Ae. aegypti* habitat, determinants from the georeferenced, scaled-up, capture point, geosampled, epidemiologic data. Moran's indices (*I*) is a way to measure geo-spatiotemporal, autocorrelation [10]. In simple terms, it's a way to quantify how closely values are clustered together in a 2-D space which is used in geography and GIS/Python/R to measure how closely clustered different features are on a map like household income, level of education, etc. To calculate Moran's I we employed

$$(N/W)*\Sigma\Sigma w_{ij}(x_i–x)(x_j–x)/\Sigma(x_i–x)2$$

where:

N: The number of county potential bird bath Ae. aegypti habitats units indexed by i and j W: The sum of all w_{ij} x: The variable of interest (zip code, predicted breeding site aquatic foci)

x: The mean of x

w_{ij}: A matrix of spatial weights

We assumed that the simple terms could quantify how closely the aggregation/non-aggregation-oriented *Ae. aegypti* habitat, determinant, geosampled, eigenized, discrete, integer values were clustered together in a 2-D space. The upper and lower bounds for our eigen-spatial filter, eigendecomposition, and model spatial matrix were constructible employing Moran's *I,* which here was given by $\lambda_{max}(n/1^T W$ 1) and $\lambda_{min}(n/1^T W$ 1) where λ_{max} and λ_{min} were the extreme eigenvalues of $\Omega = HWH$. An autocorrelation plot was generated.

3. Results

Initially, a misspecification perspective for the asymptotical, potentially eigenizable, scalable, capture point, sentinel site, county-level, signature, *Ae. aegypti,* Sentinel-2, signature model was generated in R assuming that the geosampled, aggregation/non-aggregation-oriented, potentially transmission-related, stratified, parameter estimator fit was (i.e., a standard regression equation). The primary function of the model generation was to identify the eigenizable autocorrelated disturbances in the stratified, aggregation/non-aggregation-oriented, georeferenced, capture point, sentinel site, hot/cold spot, and stratified determinants. The Graph mapping functionality in R allowed us to create choropleth, prism, block, and surface maps. The stratified latent coefficients were optimally decomposed into a white-noise component, and a set of unspecified and misspecified, model outputs that had structure. White noise is a univariate or multivariate discrete-time stochastic process, whose terms are independent and identically distributed (i.i.d.) with a zero mean [Stein. 1999]. The Annotate facility enabled us to generate a special dataset of graphics commands from which we created the stratified, county-level, *Ae. aegypti*, Sentinel-2, signature, determinant, vulnerabilityoriented, graphic, model output. The annotated output generated multiple, customized, topographic, capture point, sentinel site, georeferenceable, county-level, zip code, gridstratified, LULC maps.

Signature quantification of the interpretive, land cover patterns was renderable from the distribution of the regressed, stratified, aggregation/non-aggregation-oriented, georeferenced, *Ae. aegypti,* bird bath, signature, determinants which in this experiment was a requirement to describe independent key dimensions of the underlying uncertainty processes in the empirical, geosampled, stratified, data capture points. We were able to define a pattern in the misspecification

term. R provided an efficient interactive tool for organizing and analyzing the stratified, aggregation/nonaggregation-oriented, hot/cold spot, *Ae. aegypti*, Sentinel-2, stratified, sentinel site, county-level, scaled-up, georeferenced, epidemiologic, data, capture points.

Next, an autoregressive spatialized model was generated employing an asymptotical, stratified variable Y, as a function of a nearby *Ae. aegypti* bird bath, explanatory, signature, wavelength regressor Y in the aggregation/nonaggregation, entomologic, hot/cold spot, scaled-up model. A capture point, county-level, stratified, potentially eigenizable, *Ae. aegypti*, bird bath specifiable, geosampled, explanatorial, indicator value I (i.e., an autoregressive response), and the residual of Y was treated as a function of a nearby geosampled Y residual (i.e., an SAR or spatial error specification). For quantitative, autoregressive, hot/cold spot, vulnerability-oriented, prognosticative, entomologic vectorarthropod modeling, the SAR model furnishes an alternative specification that frequently is written in terms of matrix W [11]. Here, the spatial covariance of the asymptotically potentially, eigenizable, aggregation/on-aggregation-oriented, empirical, stratified, epidemiologic, capture point, sentinel site, hot/cold spot, scalable, georeferenceable, *Ae. aegypti,* bird bath data was a function of the matrix where T denoted the matrix transpose. The resulting matrix was symmetric and was considered a second-order specification as it included the product of two spatial structure matrices.

Euclidean distances between the georeferenced capture point, sentinel site, scaled-up, county-level, stratified, aggregation/non-aggregation-oriented, Sentinel-2, habitat determinants were definable in terms of an n-by-n geographic weights matrix, C, whose values were, 1 if the geosampled, county-level, hot/cold spot geolocations i and j were deemed nearby, and 0 otherwise. Adjusting this matrix by dividing each row entry by its row sum subsequently rendered C1, where 1 was an n-by-1 vector of ones which converted the regression-based matrix to matrix W. The resulting SAR model specification with no geosampled, scaled-up, capture point, signature determinants (i.e., the pure spatial autoregression specification) subsequently took on the following form: where was the scalar conditional mean of Y, and was an n-by-1 error vector whose parameters were statistically individually identified and normalized random variates. Spatial autoregressive models are fit using datasets that contained observations on geographical areas or on any units with a spatial representation [Cressie 2015]. Approximate standard errors for the stratified, county-level, eigenizable, *Ae. aegypti*, bird bath, georeferencable signature, determinant specifiable, vulnerability model was computable as the square roots of the diagonal elements of the estimated covariance matrix. The covariance matrix for analyzing the estimator determinants was expressible employing where designated calculus of expectations, I was the n-by-n identity matrix denoting the matrix transpose operation and was the asymptotical error variance [i.e., the variance of how far the geosampled, non-homogeneous, aggregation/nonaggregation-oriented prognosticated,

stratified, *Ae. aegypti*, bird bath-related, signature estimator determinants were spread out, eco-geographically and geo-hydrologically].

Subsequently, we employed a Hessian matrix for quantitating the empirical, georeferenced, county-level, geosampled signature habitat dataset of stratified, scaled-up, hot/spot, capture point, sentinel site, aggregation/nonaggregation-oriented evidential, observational, entomologic prognosticators. In mathematics, the Hessian matrix or Hessian is a square matrix of second-order partial derivatives of a function [Binmore and Davies, 2007]. This matrix described the local curvature of a function of the scaled up, capture point, sentinel site, *Ae. aegypti*, bird bath-related, stratified, geosampled, potentially eigenizable, estimator determinants. Given the function, if all second partial derivatives of f existed and were continuous over the domain of the function, then the Hessian matrix of f in the prognosticative, epidemiologic, signature, determinant, vulnerability-oriented, county-level, *Ae. aegypti*, bird bath model was derivable from where and were the differentiation operator with respect to the i-th argument. The matrix rendered in R was. We noted the determinant of the matrix in our scaled-up, entomologic, capture point, sentinel site, prognosticative model was Hessian. In image analysis, the Hessian matrix can describe the second-order variations of local image intensity [i.e., seasonal, aggregation/nonaggregation-oriented, stratified geolocation around a scaledup, capture point, sentinel site, LULC, reflectance pixel], thereby encoding the shape information [see Jacob et al. 2017]. In practice, it is computable by convolving an image with second derivatives of the Gaussian kernel in the x- and y-directions. Here, the matrix described the local curvature of the spatial structures over a whole county. Hessian matrix is suitable for entomologic, county-level, capture point, sentinel site, hot/cold spot, and shape detection. For our purposes, this Gaussian kernel was assumed to have a standard deviation of 1, applied on each pixel in a capture point, satellite, Sentinel-2 10m spatial resolution, *Ae. aegypti*, georeferenced sentinel site image so that the Hessian matrix was expressible as $Hf = HxxHxyHyxHyy$.

In this experiment, the Hessian matrix was relatable to the Jacobian matrix. In vector calculus, the Jacobian matrix of a vector-valued function of several variables is the matrix of all its first-order partial derivatives [10]. When this matrix is square, that is, when the function takes the same number of variables as input, the number of vector components of its output, is referred to as the Jacobian determinant [Cressie 2015]. Both the matrix and the determinant are often referred to simply as the Jacobian in the literature.

The Jacobian of a vector-valued function in the georeferenced, *Ae. aegypti*, Sentinel-2, bird bath habitat, signature determinants generalized the gradient of a scalarvalued function which in turn generalized the derivative of a scalar-valued function of every stratified, geosampled, discrete integer value in the empirical satellite waveband dataset. In other words, the Jacobian matrix of a scalarvalued

function in the prognosticative, entomologic, risk model (the transpose of) was its gradient and the gradient of a scalar-valued function of a single, scaled-up, georeferenceable, aggregation/non-aggregation-oriented, capture point, sentinel site, county-level, habitat signature prognosticator was its derivative. Further, at each sentinel site where a function was differentiable, the Jacobian described the amount of "stretching", "rotating" or "transforming" that the function imposed locally near that habitat capture point. For example, here (x′, y′) = f(x, y) was employed to smoothly transform a stratified, georeferenced, scaled-up, signature related, bird bath, habitat, wavelength, reflectance observational, evidential prognosticator in the Jacobian matrix Jf(x, y) which here described how the geosampled, county-level, determinant in the Ae. aegypti, model performed.

The hot/cold spot residuals represented independent, sentinel site, county-level, stratifiable, prognosticative, variable, clustering tendencies. The spatial pattern in the eigen-orthogonalized eigenvectors was synthetic. In the county-level, predictive, eigenvector, hot/cold spot, risk model, positive, global, eigen-autocorrelation in the local patterns of the Ae. aegypti habitat, determinants exhibited only positive local eigen-autocorrelation and vice versa for negative global eigen-autocorrelation. The eigenvectors e and ej within each set of eigenvectors were mutually eigenorthogonal employing symmetry transformation $\frac{1}{2}(V + V)$ which in this experiment was expressible employing a quadratic form as revealed in Equations (2.1) and (2.2).

The eigen-spatial filter eigendecomposed eigenvectors of specification (2.1) were eigen-orthogonal to the georeferenced, geosampled, aggregation/non-aggregationoriented, county-level, hot/cold spot, X of the regressionrelated, epidemiologic, prognosticative, signature model constructed in R employing the transmission-oriented, operationalizable, stratified, scalable, sociodemiographic and environmental, eigenized, determinants.

Conversely, the interpolatable, eigenvectors of specification (2.2) were eigen-orthogonal only to the constant unity vector 1 in X. This eigen-orthogonality had implications for predictive modeling geospatial misspecification terms in our stratifiable, vector arthropod, habitat-related, aggregation/non-aggregation-oriented, georeferenceable, transmission-oriented, vulnerability, county-level model as they allow linking each collection of eigen-orthogonalizable eigenvectors to its specific autoregressable model residuals by letting E_{SAR} be a matrix whose vectors are subsets of $\{e1, \boxtimes, en\}$SAR. Here we considered also within-group estimation of higher-order, autoregressive, panel models employing the georeferenced, clustering/non-clustering, vulnerability-oriented regressors and fixed effects where the lag order was possibly misspecified. Even when disregarding the misspecification bias, the fixed-effect bias formula regressed differently from the correctly specified case though its asymptotic order remained the same under stationarity. A linear combination of this subset was approximatable by employing the misspecification term of the simultaneous autoregressive version of the vulnerability-oriented, Ae. aegypti bird bath stratified, prognosticated, signature model

output which was expressible as $(ESAR\gamma \approx \sum_{k}^{\infty} =1\ kvk\varepsilon)(2.3)$.

The linear combination ESAR remained eigen-orthogonal to the geosampled exogenous variables X and, consequently, the estimated geosampled, sociodemographic, and environmental, stratified, predictor variable ^ were unbiased. Further, as a property of the ordinary least squared [OLS] estimator, the approximated term ESAR γ was also eigenorthogonal to the model residuals $\hat{\varepsilon}$. The model $y = X\beta + E$SAR$\hat{\gamma} + \hat{\varepsilon}$ decomposed the eigenized, stratified, prognosticative Ae. aegypti habitat, determinants y into a systematic trend component, a stochastic signal component, and white-noise residuals. The term ESAR $\hat{\gamma}$ removed variance inflation in the mean square error [MSE] term attributable to latent, eigen-autocorrelation in the scalable, aggregation/nonaggregation-oriented, geosampled, county-level, stratified, prognosticated, capture point, sentinel site, eigenized, habitat, signature, estimator determinants.

Alternatively, for the spatial lag model (2.3), an aggregation/non-aggregation-oriented, autoregressive, predictive, vulnerability-oriented, signature model was constructible employing E_{Lag} which was a matrix of those eigen-spatial filter eigenvectors that were a subset of $\{e_1, \boxtimes, e_n\}$Lag. The approximation of the misspecification term became $E_{Lag\,\gamma} \approx \sum_{k=0}^{\infty}(X\beta + \varepsilon)$. Since $E_{Lag\,\gamma}$ was correlated with the variables X, its incorporation into the scaled-up, capture point, sentinel site, county-level, stratified, risk model corrected the bias of estimated plain OLS parameters $\hat{\beta}$ in the latent, spatial lag, eigen decomposed, hot/cold spot model, summary diagnostics. The model $y = X\beta + E_{Lag\hat{\gamma}} + \hat{\varepsilon}$ was constructible from the geosampled, aggregation/non-aggregation-oriented, vulnerability-oriented, determinants which in this experiment was derivable from an eigen decomposition of the spatial lag model, However, for the georeferenced, scaled-up, capture point, hot/cold spot, geosampled, county-level, prognosticative model, eigenized, estimator determinants we noted that the trend and the timeseries, signals were no longer uncorrelated and the MSE was deflated.

The set of eigenvectors $\{e_1, \boxtimes, e_n\}$Lag of the spatial lag model (2.3) was calculable in R independent of the georeferenced, county-level, eigendecomposed, prognosticative variables X. This calculation was dependent on the underlying spatial link matrix V. We found that this eigen-spatial filtering approach was more adaptable to an exploratory specification search of the relevant stochastically interpolatable, geosampled, county-level, Ae. aegypti habitat, signature, estimator determinant, capture point, scalable, georeferenced, sentinel site, hot/cold spots. Spatial predictions rather than with the regressed temporal shifting, georeferenced, sociodemiographic and environmental, prognosticated, aggregation/non-aggregation-oriented, geosampled, explanatory, eigenized, estimator determinant, discrete values in the epidemiologic, prognosticated, risk model output were quantifiable. In contrast, for the simultaneous autoregressive model (2.2), the eigenvectors $\{e_1, \boxtimes, e_n\}$SAR depended through the projection of $M(x)$ on the approximated explanatory variables X. Thus, any change

in the underlying model structure required a recalculation of the eigen-orthogonalized, eigen-spatial, filters, for generating robust tessellations. Eigen-spatial filtering of either the spatial lag model or the simultaneous autoregressive model with a common factor constraint, thereafter, only required identification of one set of selected, eigenvectors, namely, E_{SA} or E_{Lag} E_{Lag}, respectively. The relevant set of eigenvectors was applied simultaneously to the multivariate, scaled-up, capture point, sentinel site, stratified, aggregation/non-aggregation-oriented, georeferenceable, and estimator determinants. For the generic autoregressive model (2.1), however, eigen-spatial filtering was applied individually to each geosampled, aggregation/nonaggregation-oriented, stratified, eigenized, signature determinant. The generic specification of autoregressive spatial models associated a specific spatial lag factor with the *y* variable and other lag factors for each additional, transmission-oriented, operationalizable, stratified, *Ae. aegypti* habitat, signature determinants. We employed the eigenvectors $\{e_1, \boxtimes, e_n\}$Lag to filter latent, non-zero, eigenautocorrelation coefficients embedded in the scaled-up, generic, county-level, georeferenced, prognosticative, capture point, risk model for each geosampled, aggregation/nonaggregation-oriented, straifiable, sentinel site, semiparameterizable, eigen-estimator determinant.

The final step was to identify suitable and parsimonious subsets of approximatable, eigen-orthogonalizable, eigenspatial filters E_{SAR} and E_{Lag} from the georeferenced, aggregation/non-aggregation-oriented, stratified, environmental and sociodemiographic, vulnerabilityoriented, *Ae. aegypti,* bird bath habitat, signature determinant model specifications (2.1) or (2.2). We assumed that a particular subset of eigen-orthogonalized eigenvectors was suitable for optimally, heuristically, optimizing, georeferenceable, aggregation/non-aggregation-oriented, hot/cold spot, scaled-up, capture point, county-level, sentinel sites if the optimizable residuals ε of the resulting eigenfunction, eigen-spatial filter, eigen-autocorrelation model became independent with respect to the underlying geosampled spatial structure *V.* Here, parsimony in the model estimation was definable as the smallest possible subset of eigen-orthogonalized eigenvectors which led to the independence in the *Ae. aegypti* habitat, forecasted, risk model, hot/cold spot, aggregation/non-aggregation-oriented, stratified, signature determinant derivatives. We noted that the patterns of different eigenvectors expressed independent and filter eigen-autocorrelation as interpreted from the model derivatives. This was formalized by an eigenized, signature determinant associated to the georeferenced, county-level, sentinel site, capture point *Ae. aegypti* habitat, stratified, hot/cold spot foci. Positive and negative, latent, eigenautocorrelation pseudo-R^2 values were subsequently reported by employing a generalized linear mixed model [GLMM] estimation results from R.

4. Discussion

In this experiment, we attempted to establish the limiting

distribution of the Moran test statistic for quantifying the independence in datasets of georeferenced, *Ae. aegypti* bird bath signature predictor variables geosampled at multiple sites in various neighborhoods in Hillsborough County. Initially, we partitioned each georeferenced capture point, *Ae. aegypti* habitat using Sentinel-2 visible and near-infra-red (NIR) data imaged, capture point georeferenced, in GIS to compare the spatial concurrence of adult-sampled mosquitoes based on a LULC reflectance signature covariate for evaluating surveillance activities. We then employed a semiparametric eigen-spatial filtering approach using a second order eigenfunction eigendecomposition algorithm based on a geographic connectivity matrix for computing the Moran's *I* statistic. The underlying rationale for employing an eigenvector eigen-spatial filtering approach for quantifying spatial autocorrelation levels is that eigenvectors that are extracted from a transformed spatial link matrix can exhibit distinctive spatial patterns [10]. The eigenvectors generated from geosampled, seasonal, georeferenced, bird bath, *Ae. aegypti* habitat data were mutually orthogonal and uncorrelated allowing for an explicit description of error in spatially lagged and simultaneous autoregressive, spectral, signature frameworks constructed from field-geosampled georeferenced entomologic, zip-code, gridded, LULC, NDVI, NDWI and 3-D DEM parameters. Contribution in literature [4, 13] has covered many factors relating to the foraging behavior of vector mosquito species by generating models based on productivity and oviposition of gravid mosquitoes. Statistical deficiencies; however, in quantifying spatial error in field-geosampled arboviral mosquito data for measuring geo-spatiotemporal productivity and predicting prolific habitats can hamper progress in implementing control strategies as outlined in Gu and Novak (2005) rendering intervention efforts for targeting productive habitats inefficient. Undiagnosed spatial autocorrelation effects in geosampled georeferenced vector mosquito data can spill over across units of observation which can result in a misspecified model (Jacob et al., 2015). Since the strategy of targeted interventions is to recognize the importance of the variation in mosquito production among breeding sites in the design of control programs for suppression of disease transmission, it is vital to statistically summarize spatial error in autoregressive, *Ae aegypti,* bird bath, signature, interpolation models. We were able to construct a robust semiparametric eigen-spatial filtering model to deal explicitly with error in spatially lagged and simultaneous autoregressive signature interpolation models for identifying prolific habitats based on field-geosampled satellite data of georeferenced *Ae. aegypti* bird bath habitats in Hillsborough County, Florida.

The NDVI *Ae. aegypti* Hillsborough County habitat map revealed geolocations of potential bird bath aquatic foci throughout different land covers in Hillsborough County. Several deterministic, signature habitat models have been developed in the literature [4, 13] to study the interactions of solar radiation within vegetation canopies of entomological, vector, arthropod, larval habitats in various sub-county abatement, geolocations e.g., hyper-arid, arid, semi-arid,

prerain, etc.), to understand how biodiversity responds to environmental degradation in various ecosystems for optimally, remotely targeting, *Ae. aegypti* seasonal, super breeder, foci. In this experiment, diversity and assemblage structure differed between amongst capture point geolocations and between LULC areas which were reclassified as territories vulnerable to *Ae. aegypti* bird bath habitats suitability. Here, NDVI measured wavelength Sentinel-2 imaged reflectance visible and NIR explanators of seasonal, hyper-larval productivity currently including canopy closure, vegetation height, percent cover of bare ground, leaf litter, and grasses amongst collected points in sub-county, abatement, LULC classified geolocations of Hillsborough County.

High-resolution NDVI, county-level signature models may be adapted to a system of simultaneous differential equations to investigate inhomogeneous, vegetation, LULC, and canopy radiation. For example, Iwamura, et. al., [2020] employed an ArcGIS deterministic model to distinguish, unmixed, directional, spectral reflectance of a capture point, LULC reclassified, vegetation, and intermittently canopied paradigm. In this experiment, effort total proportion of spectral reflection absorbed by the canopy system changed as a function of the solar zenith angle; the total global reflected spectral also changed. The solar zenith angle is the angle between the zenith and the center of the Sun's disc [Jensen 2015]. The deterministic models simulated the apparent reflectance in multiple, satellite data (Sentinel-2 at 10 m resolution) unmixed, LULC wavebands above the canopy, and this reflectance revealed varying solar zenith angles due to geometrical-radiation, signature interactions within the capture point, zip code grid-stratified, canopied LULCs. Many epi-entomological, vector arthropod NDVI studies for identifying unfamiliar prolific foci do not distinguish between unmixed, LULC capture point, global and directional, interpolative, unmixed, canopy, reflectance factors, (i.e., RGB sub-pixel, frequencies). This distinction here dictates the nature of the friability of georeferenceable, sub-county abatement, capture point, canopy-vegetated, bird bath, *Ae aegypti*, larval habitat, unmixed, spectral, signature radiance for identifying, unsampled, hyperproductive, seasonal, vegetated breeding sites in a stochastic iterative interpolation.

Zip code stratified LULC reflectance, seasonal traits can dictate the nature of real-time, imaged, capture point, *Ae aegypti*, habitat, wavelength, reflectance alternativeness, and interrogatability. Such tactics within a real-time interactive iOS dashboard may allow categorizing temporal, resampled, RGB frequencies seasonal time frame for optimally geolocating unknown, unsampled, sub-county abatement, potential, and super breeder foci. Understanding the vertical pattern of LULC traits across residential homestead plant canopies may provide critical information on ecosystem functioning and structure and responses to climate change associated with seasonal, *Ae. aegypti* breeding site aquatic foci.

The impact of vertical canopy position NDWI on unmixed, leaf spectral NDVI properties and subsequently leaf traits across the entire spectrum for a, sub-county abatement,

potential, seasonal, super breeder, bird bath, *Ae. aegypti,* larval habitat is poorly understood. Real-time, dashboard, optical properties may track variability in leaf traits across, a bird bath, *Ae aegypti,* LULC eco-georeferenced, capture point, and generate a vertical canopy profile using Partial Least Square Discriminatory Analysis (PLS-DA) in a realtime, dashboard, ArcGIS or python module. In so doing, leaf spectral measurements together with leaf traits (nitrogen, carbon, chlorophyll, equivalent water thickness, and specific leaf area) may be studied at multiple, seasonal, vertical, canopy positions along the plant stem: lower, middle, and upper employing LULC, NDWI and NDVI Sentinel-2 maps. Observing, real-time, mappable remotely captured, foliar nitrogen (N), chlorophyll (Cab), carbon (C), and equivalent water thickness (EWT) may reveal, higher concentrations in the upper canopy leaves compared with lower shaded leaves in a potential, seasonal, *Ae. aegypti*, bird bath capture point, larval habitat, sub-county abatement, classified LULC, aquatic foci. Plants exhibit higher nutrient stoichiometry in the upper illuminated leaves that receive higher photon flux density compared to lower canopy-shaded leaves [26].

The eigendecomposition, eigen-spatial filtering approach added a minimally sufficient set of eigenvectors as proxy variables to the set of evidential, observational, *Ae. aegypti* birdbath, capture point, sentinel site, prognosticators in the county-level, signature determinant, vulnerability-oriented, vector arthropod model by inducing mutual independence in the scaled-up, capture point, sentinel site, county-level, geosampled, potentially georeferenced, signature estimator determinants in eigenvector eigen-geospace. The hot/cold spot *Ae. aegypti* birdbath, capture point, sentinel site, residuals represented independent, sentinel site, county-level, stratifiable, prognosticative, variable, clustering tendencies. The spatial pattern in the eigenvectors was synthetic. At the county level, predictive, *Ae. aegypti* birdbath, capture point, sentinel site hot/cold spot, risk model, positive, global, eigenautocorrelation in the local patterns of the parameters exhibited only positive local eigen-autocorrelation and vice versa for negative global eigen-autocorrelation. The eigenvectors e_i and e_j within each set of eigenvectors were mutually eigen-orthogonalizable employing symmetry transformation $\frac{1}{2}(V + V^T)$ which in this experiment was expressible employing a quadratic form as revealed in Equations (2.1) and (2.2).

As mentioned previously, the eigen-spatial filter eigendecomposed eigenvectors of specification (2.1) were eigen-orthogonal to the georeferenced, geosampled, aggregation/non-aggregations-oriented, county-level, hot/cold spot, X of the regression-related, epidemiologic, prognosticative, county-level, specified, *Ae. aegypti* birdbath, capture point, sentinel site, signature determinant, the model constructed employing the operationalizable, stratified, scalable, sociodemographic and environmental, eigenized, signature determinants. Conversely, the interpolatable, eigenvectors of specification (2.2) were eigen-orthogonal only to the constant unity vector 1 in X. This eigenorthogonality had implications for predictive signature modeling geospatial misspecification terms in our stratifiable, *Ae. aegypti* birdbath,

capture point, sentinel site aggregation/non-aggregation-oriented, georeferenceable, risk model as they allow linking each collection of eigenorthogonalized eigenvectors to its specific autoregressable county-level, signature, model residuals by letting E_{SAR} be a matrix whose vectors are subsets of $\{e_1, \boxtimes, e_n\}SAR \cdot$. Here we considered also within-group estimation of higher-order, autoregressive, panel signature models employing the stratified, georeferenced, time series, dependent, clustering/non-clustering, vulnerability-oriented *Ae. aegypti* birdbath, capture point, sentinel site regressors and fixed effects where the lag order was possibly misspecified. Even when disregarding the misspecification bias, the fixed-effect bias formula regressed differently from the correctly specified case though its asymptotic order remained the same under stationarity. A linear combination of this subset was approximatable by employing the misspecification term of the simultaneous autoregressive version of the vulnerabilityoriented, habitat-related, stratified, prognosticated, model output which was expressible as $E_{SAR\ \gamma} \approx \sum_{k=1}^{\infty} \rho^k V^k \varepsilon)$ (2.3).

The linear combination $E_{SAR\gamma}$ remained eigen-orthogonal to the geosampled exogeneous *Ae. aegypti* birdbath, capture point, sentinel site, signature variables X and, consequently, the estimated dependent, geo-sampled, sociodemographic, and environmental, stratified, predictor variables $\hat{\beta}$ were unbiased. Further, as a property of the OLS estimator, the approximated term $E_{SAR\ \gamma}$ was also eigen-orthogonal to the model residuals $\hat{\varepsilon}$. The model y = X$\hat{\beta}$ + $E_{SAR\hat{}\gamma}$ + $\hat{\varepsilon}$ decomposed the, eigenized, *Ae. aegypti* birdbath, capture point, sentinel site, stratified variable y into a systematic trend component, a stochastic signal component, and whitenoise residuals. The term $E_{SAR\ \hat{}\gamma}$ removed variance inflation in the mean square error term attributable to latent, eigenautocorrelation in the scalable, aggregation/non-aggregationoriented, geosampled, county-level, stratified, prognosticated, vector arthropod-related, capture point, sentinel site, eigenized determinants.

Alternatively, for the spatial lag model (2.3), an aggregation/non-aggregation-oriented, autoregressive, predictive, vulnerability-oriented, *Ae. aegypti* birdbath, capture point, sentinel site, the model was constructible employing E_{Lag} which was a matrix of those eigenorthogonalized eigen-spatial filter eigenvectors that were a subset of $\{e_1, \boxtimes, e_n\}Lag$. The approximation of the misspecification term became $E_{Lag\ \gamma} \approx \sum_{k=0}^{\infty} \rho^k V^k (X\beta + \varepsilon)$.

Since $E_{Lag\ \gamma}$ was correlated with the variables X, its incorporation into the scaled-up, capture point, sentinel site, county-level, stratified, risk model corrected the bias of estimated plain OLS parameters $\hat{\beta}$ in the latent, spatial lag, eigen-spatial filter, hot/cold spot, eigenized, estimator, vulnerability-oriented, summary diagnostics in R. The model $y = X\beta + E_{Lag\ \hat{}\gamma} + \hat{\varepsilon}$ was constructed from the geosampled, aggregation/non-aggregation-oriented, *Ae. aegypti*, bird bath habitat vulnerability-oriented, signature determinants which in this experiment was derivable from an eigendecomposition of the spatial lag model, However, for the georeferenced,

scaled-up, capture point, hot/cold spot, geo-sampled, countylevel, prognosticative model, eigenized, *Ae. aegypti*, bird bath habitat estimator determinants we noted that the trend and the signature wavelength Sentinel-2 reflectance signals were no longer uncorrelated, and the mean square error was deflated.

The set of eigenvectors $\{e_1, \boxtimes, e_n\}$ Lag of the spatial lag model (2.3) was calculable in R independent of the georeferenced, county-level, eigendecomposed, prognosticative variables X. This calculation was dependent on the underlying spatial link matrix V. We found that this eigen-spatial filtering approach was more adaptable to an exploratory specification search of the relevant stochastically interpolatable, county-level, *Ae. aegypti* birdbath, capture point, sentinel site, capture point, scalable, georeferenced, sentinel site, hot/cold spots, and spatial predictions rather than with the regressed temporal shifting, sociodemographic and environmental, prognosticated, aggregation/nonaggregation-oriented, geo-sampled, explanatory, eigenizable, estimator determinant, discrete values in the epidemiologic, prognosticated, risk model output. In contrast, for the simultaneous autoregressive model (2.2), the eigenvectors $\{e_1, \boxtimes, e_n\}SAR$ depended through the projection of $M(x)$ on the approximated explanatory variables X. Thus, any change in the underlying model structure required a recalculation of the eigen-orthogonalized, eigen-spatial, filters, for generating robust tessellations. Eigen-spatial filtering of the spatial lag *Ae. aegypti* birdbath, capture point, sentinel site, model, or the simultaneous autoregressive model with a common factor constraint, thereafter, only required identification of one set of selected, eigenvectors, namely, E_{SAR} or E_{Lag}, respectively. The relevant set of eigenvectors was applied simultaneously to the multivariate, scaled-up, capture point, sentinel site, stratified, aggregation/non-aggregation-oriented, georeferenceable, and signature determinants. For the generic autoregressive model (2.1), however, eigen-spatial filtering was applied individually to each geosampled, aggregation/non-aggregation-oriented, *Ae. aegypti* birdbath, capture point, sentinel site, stratified, signature determinant. The generic specification of autoregressive spatial models associated a specific spatial lag factor with the y variable and other lag factors for each additional, operationalizable, stratified, *Ae. aegypti* habitat geosampled signature determinants. We employed the eigenvectors $\{e_1, \boxtimes, e_n\}Lag$ to filter latent geo-spatiotemporal, non-zero, eigenautocorrelation coefficients embedded in the scaled-up, generic, county-level, georeferenced, prognosticative, capture point, risk model for each aggregation/non-aggregationoriented, straifiable, sentinel site, semi-parameterizable *Ae. aegypti* birdbath, capture point, sentinel site, eigen-estimator determinant.

The *Ae. aegypti* birdbath, capture point, sentinel site, model forecasts identified suitable and parsimonious subsets of eigen-orthogonalizable, eigen-spatial filters E_{SAR} and E_{Lag} from the georeferenced, aggregation/non-aggregationoriented, stratified, environmental and sociodemographic, vulnerability-oriented, *Ae. aegypti* birdbath, capture point,

sentinel site, model specifications (2.1) or (2.2). We assumed that a particular subset of eigen-orthogonalized eigenvectors was suitable for optimally, heuristically, optimizing, georeferenceable, aggregation/non-aggregation-oriented, hot/cold spot, scaled-up, capture point, *Ae. aegypti* birdbath, capture point, sentinel site, county-level, sentinel sites if the optimizable residuals $\hat{\varepsilon}$ of the resulting eigenfunction, eigenspatial filter, the eigen-autocorrelation model became independent with respect to the underlying geo-sampled spatial structure *V*. Here, parsimony in the model estimation was definable as the smallest possible subset of eigenorthogonalized eigenvectors which led to the independence in the geo-spatiotemporal, *Ae. aegypti* birdbath, capture point, sentinel site, prognosticated, risk model, hot/cold spot, aggregation/non-aggregation-oriented, stratified, estimator, determinant derivatives. We noted that the patterns of different eigenvectors expressed independent and filter eigenautocorrelation as interpreted from the model derivatives. This was formalized by an estimator determinant associated to the georeferenced, sentinel site, capture point, *Ae. aegypti* birdbath, capture point, sentinel site, hot/cold spot countylevel, foci. Positive and negative, latent, eigenautocorrelation pseudo-R^2 values were subsequently reported by employing GLMM estimation results from the R summary diagnostics.

Advances in the various semiparametric eigen-Bayesian, algorithmic Markovian, prognosticative, general autoregressive conditional heteroscedastice [GARCH] signature models may prove to be effective for geospatiotemporally quantitating the reflectance bias introduced by microstructure noise in georeferenceable, time series dependent, aggregation/non-aggregation-oriented, countylevel, stratifiable, *Ae. aegypti*-related, bird bath, capture point, sentinel site, scalable, signature determinants in an empirical geosampled arboviral dataset. A stochastic process is called Markovian if at any time t the conditional probability of an arbitrary future event given the entire past of the process—i.e., given X(s) for all s≤t—equals the conditional probability of that future event given only X(t). They may be extendable into nonlinear patterns, including the exponential GARCH (EGARCH), heterogeneous, autoregressive GARCH (HAR-GARCH), and threshold GARCH (TGARCH) models. These models with skew Student's t-distribution may be applicable for optimally, heuristically, optimizing, targeting, and prioritizing, aggregation/non-aggregation, georeferenceable, epidemiologic, *Ae.aegypti*-related, stratifiable, county-level, hot/cold spots, and their signature determinants. EigenBayesian, algorithmic, Markvian GARCH estimations can be constructed with all major software packages and with many numerical general-purpose platforms. In fact, for R alone there exist several packages that could be employed for prognosticative, epidemiologic, scalable, stratifiable, county or district-level, *Ae.aegypti*-related, bird bath signature determinant, eigen-Bayesian, Markovian algorithmic, GARCH, forecast modeling.

In future research, we may generate a fully eigen-Bayesian probabilistic matrix factorization model in which model capacity is controlled automatically by integrating over the empirical geo-sampled dataset of county-level, georeferenceable, submeter-resolution [Worldview 4, 46 centimeter visible and NIR spatial resolution], imaged *Ae. aegypti* habitat model parameters and hyperparameters. We may introduce priors for the hyperparameters and maximize the log-posterior of the model over both the parameters and hyperparameters, which may allow the *Ae aegypti*, bird bath habitat model complexity to be controlled automatically based on the training data [i. hyper/hypo-endemic, capture point, sentinel site, scaled-up, county-level, epidemiologic, aggregation/non-aggregation-oriented, capture point, sentinel site, eigenized, estimator determinants]. Though this approach has been shown to work in practice it is not wellgrounded theoretically hence it does not occur in the literature, however, we may employ this joint optimization technique to predictively geolocate, eigenBayesian, eigendecomposed, county-level, geo-referenceable, hyper/hypo-endemic, aggregation/non-aggregation, *Ae, aegypti,* stratifiable, eigen-spatial filter, estimator, determinant, capture points.

We may begin with a "prior distribution" based on the relative likelihoods of the geosampled, sociodemographic, environmental, stratified, eigenized, time series, dependent, *Ae, aegypti,* habitat signature determinants. In practice, it is common to assume a uniform distribution over the appropriate range of values for the prior distribution [3]. Next, a research team calculated the likelihood of the observed asymptotical distribution as a function of the eigen-estimator, determinant, semi-parameterized, capture point, sentinel site, scalable county-level, stratified, discrete, integer values by multiplying the likelihood function by the prior distribution which may be subsequently normalized to obtain a unit probability over all possible geosampled, independent, signature determinant, unmixed, discrete, integer values (i.e., posterior distribution). The mode of the distribution approximated probability intervals in the empirical, signature determinant, geosampled dataset. In eigen-Bayesian inference, a probability interval is a probabilistic region around a posterior moment and is similar in use to a frequentist confidence interval (Jacob et al. 2023). An eigenBayesian model may capture spatial heterogeneity in an entomological, eco-epidemiological, vector, arthropod, submeter resolution signature resolution, model which may, in turn, reveal variation or instability in observational units (e.g., gridded, geo-referenceable discontinuously canopied, *Ae aegypti,* oviposition, bird bath, capture points) across a county region (high socioeconomic, neighborhood, agroirrigated floodplain) which may imply that the functional forms and/or behavioral parameters vary by LULC classified geolocation.

The adaptation for oviposition preference may have been part of the overall evolution of domesticity that likely occurred in North Africa when ancestral sylvan *Ae. aegypti* became isolated from sub-Saharan Africa due to the Sahara Desert [30]. In general, oviposition choice in mosquitoes is mainly due to volatiles produced by the microorganisms in the larval (Yelfwagash et al. 2017). Thus, as long as appropriate volatiles are produced by a standing urban commercial/residential or rural commercial/residential rural

sparsely canopied artificial pool of water, an opportunistic species like *Ae. aegypti* may oviposit there. This is supported by situations where this domestic form outside Africa has reverted to developing in natural water. The results from this study provided a total of 50 predicted habitat geolocations of the *Ae. aegypti* mosquito throughout Hillsborough County, Florida, which when placed upon Uelmen et al.'s abundance hotspot model of *Ae. aegypti* aligned with the areas of high abundance gave us a more precise location of these habitats [27].

The climate and geophysical characteristics of the basin (such as topography and vegetation) and anthropogenic activities are the main factors influencing the ecohydrological biophysical processes in urban and nonurban basins. Thus, a seasonal LULC eco-cartographic realtime data management system may be able to determine determinants that influence the evolution of the surface of these basins (and hence any *Ae. aegypti* bird bath, immature, habitat, oviposition, capture point geosampled at the basin), will depend on retrieving geo-spatiotemporal capture point, sentinel site patterns of the precipitation and evaporation rates. The distribution of rainfall is one of the favorable factors that can influence the number of *Ae. aegypti* mosquito. Amongst the remotely sensed, high resolution, LULC, signature interpolation models, becoming well-established models for analyzing the impact of land management practices on water, sediment, and agricultural chemical yields in large complex watersheds, which can influence *Ae. aegypti*, immature, habitat, oviposition, capture point.

Previous studies have collected *Ae. aegypti* abundance data via traps (BG-Sentinel, CDC light traps, suction, and Wilton) which allowed them to create heat maps that describe the population range of the mosquito throughout the county [27]. This data has allowed abatement districts to see population trends over the years, allowing them to focus their control efforts in areas that see higher mosquito populations in the peak seasons. This collection of data has been extremely useful in terms of mapping where the *Ae. aegypti* habitats tend to be in a general sense, which this paper used to validate our predicted habitats when comparing to Uelmen et al.'s results, which displayed a hot and cold spot map of the *Ae. aegypti*'s abundance within the Tampa Bay Area, FL, many of our predicted habitats aligned with their confirmed habitat areas that they found [27]. Our model's diagnostic field summary data revealed sensitivity and specificity approaching 100%.

Worldview [Wv] 4 relatively high spatial resolution (~46 cm) image data may be usable to define potential frequency increases in the duration of heat waves due to climate changes throughout Hillsborough County urban centers and agro-pastureland migrant farm worker communities. Spectral signatures may be generated using Wv-4data of surface temperature, NDVI, NDWI, LULC, etc. Future research efforts should incorporate daily GRIDMET gridded point data of weather variables such as maximum air temperature, relative humidity, and precipitation in the county. Wv-4 data may be photogrammetrically processed to derive a 3dimensional Digital Elevation [DEM.] for determining watershed catchment variables and slope coefficients of ground-referenced *Ae. aegypti* bird bath, capture points that may be applicable to retrieve the land surface temperature (LST) distribution. The spatial pattern of LST in the Hillsborough County area may be retrieved to characterize their local effects on urban heat islands. In addition, the correlation between LST and the NDVI may be analyzed to explore the impacts of the green land [e.g., high-income urban parks, farmlands, grasslands, swamps, wetlands, etc.] and the built-up land on the heat islands by calculating the geoecological evaluation index of sub-urban region. Future research on *Ae. aegypti* birdbaths should include interpolation of the ground reference points of the meteorological variables using a Bayesian Maximum Likelihood Classifier [MLC] over a land use/land cover classified Hillsborough County map to determine a vulnerability index at the gridded zip code level using census data in Python.

Combining artificial intelligence (AI) machine learning classifiers and interpolative ArcGIS [geo-AI] in an interactive, dashboard configurable, web-friendly smartphone application (app) may aid in optimally scaling up sentinel site capture points for predictively mapping unknown, countylevel, *Ae. aegypti* birdbaths, larval habitat, seasonal occurrence, abundance, and distribution. By employing realtime, unmanned aerial vehicles [UAV] or drones, real-time retrievable capture points, sentinel sites, wavelength, reflectance datasets of seasonal, imaged, high-resolution LULC classified, *Ae. aegypti* birdbaths larval habitat characteristics [e.g., water situation (turbid or clean, stagnant, or running), substrate type, (e.g., moist, or dry), site type (man-made or natural), sunlight situation, site situation (transient or permanent, with or without vegetation), etc.] a geo-referenceable, RGB, signature may be generatable employing geo-AI technologies infused into an iOS smartphone application [app]. This protocol has been employed to identify the aquatic sources for Black Fly larvae and pupae in West and East Africa (Cameroon and Uganda, respectively) as well as the potential geolocations for immature (larval) habitat sources of Chrysop species the vector of Loa Loa. Since these model systems are built on spectral signatures of habitats and employ a real-time larval source management system for geolocating those areas where seasonal, vector arthropod, larval habitat population is the most concentrated, immobile, and accessible, this method has several ramifications regarding its biological utility as a realtime tool for surveillance and monitoring the implementation of control applications by prioritization of nuisance. The sites in question could be specifically identifiable by georeferencable capture points and subsequently scaled up and treated via real-time dashboard technology or by standard mosquito operational tactics depending on the site's landscape. In addition, this system could also provide the specific geolocation for adult emergence, forecasting the where, when, and time to initiate an adult control operation. Thus, individuals would be treated before they disperse, and when the adult population is highly concentrated predispersal.

Some suggested solutions would be integrating Jacob et al.'s "Seek and Destroy" intervention method, which, within 31 days, was able to eliminate all *Anopheles* larval habitats in the Gulu district of Northern Uganda [14]. Similar to his intervention, we will train abatement district officers to map potential habitats using ArcGIS and Python. We can create an application [app] that displays real-time mosquito habitat data that can serve as a centralized reporting system. For those who own bird baths in their yards, we suggest flipping or flushing bird baths once or twice a week. Changing the water has been a long-time suggestion of many abatement districts, but upping the frequency can disrupt the larval cycle of *Ae. aegypti*.

5. Limitations

We used sentinel-2 10 m data, but we would like to use world-view 1 panchromatic 31 cm spatial resolution because it would allow us more discrimination of a capture point sentinel site – *Ae. aegypti* habitat. Predicted *Ae. aegypti* Habitats may have visual discrimination of the capture point of the habitat, we were not able to confirm water levels or water clarity in the capture point since it was on private property. We did not conduct larval tests. We did not use any tactics that involved image-based AI. However, in my following publication, I will incorporate a convulsion neural network infused into a smartphone dashboard application (app). This interactive app will be able to conduct all satellite data analysis, including land cover classification generation of elevation maps, generation of vegetation maps, and construction of autocorrelation matrixes. We would also like to implement a Bayesian probabilistic periodical model to determine significant levels of determinants associated with *Ae. aegypti* habitats. Further, we would like to incorporate a time series autoregressive error model (GARCH) to determine any violations of regression assumptions (multicollinearity, non-Gaussian error variance, etc.).
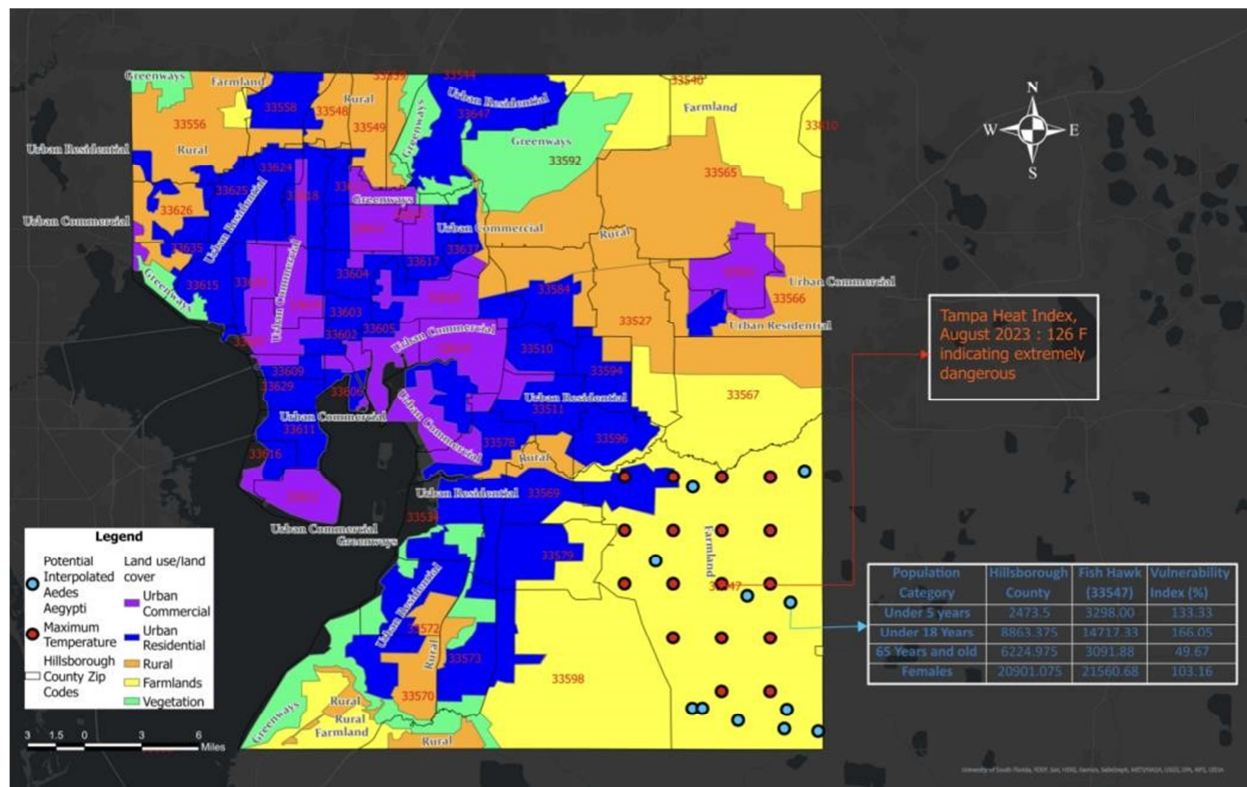

Figure 7. Vulnerability Index map of Ae. aegypti in rural parts of Hillsborough County, FL.

6. Conclusion

In conclusion, a Sentinel-2, RGB signature of a georeferenced, capture points, bird bath habitat can be interpolated in Python which can map unknown aquatic breeding site foci of *Ae. aegypti*. These maps can allow local vector control abatement district officers to implement a larval source management program targeting zip code, grid stratified, and geolocations of seasonal *Ae. aegypti* bird bath habitats.

Conflicts of Interest

The authors declare no conflicts of interest.

References

[1]   Al-Rashidi, H. S., Alghamdi, K. M., Al-Otaibi, W. M., AlSolami, H. M., & Mahyoub, J. A. (2022) Effects of blood meal sources on the biological characteristics of Ae. aegypti and Culex pipiens (Diptera: Culicidae). Saudi Journal of Biological Sciences. 29(12). Doi: 10.1016/j.sjbs.2022.103448.

[2]   Cornel AJ, Holeman J, Nieman CC, Lee Y, Smith C, Amorino M, et al. Surveillance, insecticide resistance and control of an invasive Aedes aegypti (Diptera: Culicidae) population in California. F1000Res. 5: e194. doi: https://doi.org/10.12688/f1000research.8107.3

[3]   Cressie, N. & Lahiri, S. N. (1993) The asymptotic distribution of REML estimators. Journal of Multivariate Analysis. 45(2), 217-233. https://doi.org/10.1006/jmva.1993.1034

[4]   Dinh E and Benjamin G. Jacob (2017) A Negative Binomial with a Non- Homogenous Gamma Distributed Mean for Robustifying Pseudo R2 Regression Values of Immature Vector and Nuisance Mosquito Count Data for Optimally Discerning Un-Geosampled Waste Tire Oviposition Sites in a Subtropical Habitat in SAS®/GIS Using Worldview-3 Visble and Near Infra-Red Data in Hillsborough County, Florida. Journal of Remote Sensing & GIS 6(7), 22-27. Doi: 10.4172/2469-4134.1000167.

[5]   Eisen, L., Moore, C. G. (2013) Aedes (Stegomyia) Aegypti in the continental United States: A vector at the cool margin of its geographic range. Journal of Medical Entomology. 50(3), 467-478. https://doi.org/10.1603/ME12245

[6]   Ern Ang, M. L., Arts, D., Crawford, D., Labatos, B. V., Ngo, K. D., Owen, J. R., Gibbins, C., Lechner, A. M. (2021) Socioenvironmental land cover time-series analysis of mining landscapes using Google Earth engine and web-based mapping. Remote Sensing Applications: Society and Environment. 21. https://doi.org/10.1016/j.rsase.2020.100458

[7]   Friend, W. G. & Smith J. J. B. (1977) Factors affecting feeding by bloodsucking insects. Annual Reviews Entomology. 22, 309-31.

[8]   Garcia-Sanchez, D. C., Pinilla, G. A., Quintero, J. (2017) Ecological characterization of Aedes Aegypti larval habitats (Diptera: Culicidae) in artificial water containers in Girardot, Colombia. Journal of Vector Ecology.

[9]   Gomroki, M., Hasanlou, M., Reinartz, P. (2023). STCDEffV2T Unet: Semi transfer learning EfficientNetV2 T-Unet network for Urban/Land Cover change detection using Sentinel-2 satellite images. Remote Sensing. 15(5), 1232. https://doi.org/10.3390/rs15051232

[10] Griffith, D. A. (2003). Spatial Autocorrelation and Spatial Filtering: Gaining Understanding Through Theory and Scientific Visualization. Advances in Spatial Science. Berlin, Heidelberg: Springer. https://doi.org/10.1007/978-3-54024806-4.

[11] Griffith, D. A. (2005) Effective Geographic Sample Size in the Presence of Spatial Autocorrelation. Annals of the Association of American Geographers. 95(4), 740-760, DOI: 10.1111/j.1467-8306.2005.00484.x.

[12] Jacob B. G., Novak, R. J., Toe, L., Sanfo, M. S., Tibgueria, R., Pare, A., Noma, M., Griffith, D., Unnasch, T. R. (2014) Denoising a model employing automated bandwidth selection procedures and pre-whitened Euclidean-based quadratic surrogates in PROC ARIMA for optimizing asymptotic expansions and simulations of onchocerciasis endemic transmission zones in Burkina Faso. Journal of Public Health and Epidemiology. 6(11), 347-389. https://doi.org/10.5897/JPHE2013.0629

[13] Jacob B. G. and Novak R. J. (2017) Gauging queryable iterative estimator uncorrelatedness from incompatibilistic propagational Poissionian noise in eigen-normalized nonnegativity constraints employing analogs of the Pythagorean theorem and parallelogram laws in sub-meter resolution pseudo-Euclidean space in C++ for semi-parametrically prognosticating synergistic semi-logarithmic Aedes aegypti non-ordinate axis-scaled landscape weightage covariances of episodical sylvatic yellow fever case distributions for an agroirrigated riceland village ecosystem in Gulu, Uganda. Journal of Advanced Mathematics. 1(3), 1-448.

[14] Jacob B. G., Loum, D., Kaddumukasa, M., Kamgno, J., Djeunga, H. N., Domche, A., Nwane, P., Mwangangi, J., Hernandez Bojorge, S., Parikh, J., Csanova, J., Izurieta, R., Michael, E., Mason, T., Mubangizi, A. (2021) Geospatial artificial intelligence infused into a smartphone drone application for implementing 'Seek and Destroy' in Uganda. American Journal of Entomology. 5(4), 921-109. Doi: 10.11648/j.aje.20210504.11.

[15] Mishra, P. K., Rai, A., Rai, S. C. (2020) Land use and land cover change detection using geospatial techniques in the Sikkim Himalaya, India. The Egyptian Journal of Remote Sensing and Space Science. 23(2), 133-143. https://doi.org/10.1016/j.ejrs.2019.02.001

[16] Mundis, S. J., Estep, A. S., Waits, C. M., Ryan, S. J. (2020) Spatial variation in the frequency of knockdown resistance genotypes in Florida Aedes aegypti populations. Parasites & Vectors. 13(241). https://doi.org/10.1186/s13071-020-04112-3

[17] Painsky A, Rosset S (2017). "Cross-Validated Variable Selection in Tree-Based Methods Improves Predictive Performance". IEEE Transactions on Pattern Analysis and Machine Intelligence, vol. 39, no. 11, pp. 2142-2153, 1 Nov. 2017, doi: 10.1109/TPAMI.2016.2636831.

[18] Machine Intelligence. 39(11), 2142–2153. https://doi.org/10.1109/TPAMI.2016.2636831

[19] Parker, C., Ramirez, D., Connelly, R. C. (2019) Statewide survey of Ae. aegypti and Aedes albopictus (Diptera: Culicidae) in Florida. Journal of Vector Ecology. 44(2), 210-215. https://doi.org/10.1111/jvec.12351

[20] Parker, C., Ramirez, D., Thomas, C., Connelly, R. C. (2020) Baseline susceptibility status of Florida populations of Ae. aegypti (Diptera: Culicidae) and Aedes albopictus. Journal of Medical Entomology. 57(5), 1550-1559. https://doi.org/10.1093.jme/tjaa068

[21] Qualls, W. A., Steck, M. R., Weaver, J. R., Zhang, Y., Xue, R., Sallam, M. F. (2021) Shift in the spatial and temporal distribution of Aedes t.

[22] Richards SL, Balanay JAG, Fields M, Vandock K (2017) Baseline insecticide susceptibility screening against six active ingredients for Culex and Aedes (Diptera: Culicidae) mosquitoes in the United States. J Med Entomol 54: 682–695. https://doi.org/10.1093/jme/tjw231

[23] Richards SL, Balanay JAG, White AV, Hope J, Vandock K, Byrd BD et al (2018) Insecticide susceptibility screening against Culex and Aedes (Diptera: Culicidae) mosquitoes from the United States. J Med Entomol 55: 398–407. https://doi.org/10.1093/jme/tjx198

[24] Stoddard, P. K. (2018) Managing Aedes aegypti populations in the first Zika transmission zones in the continental United States. Acta Tropica. 187, 108-118. https://doi.org/10.1016/j.actatropica.2018.07.031

[25] Throngsripong, P., Hyman, J. M., Kapan, D. D., Bennett, S. N. (2021) Human-Mosquito Contact: A missing link in our understanding of mosquito-borne disease transmission dynamics. Annals of the Entomological Society of America. 114(4), 397-414. https://doi.org/10.1093/aesa/saab011

[26] Trewin, B. J., Darbro, J. M., Jansen, C. C., Schellhorn, N. A., Zalucki, M. P., Hurst, T. P., Devine, G. J. (2017) The elimination of the dengue vector, Ae. aegypti, from Brisbane, Australia: The role of surveillance, larval habitat removal and policy. PLoS Negl Trop Dis 11(8): e0005848. https://doi.org/10.1371/journal.pntd.0005848

[27] Tucker, C. J. (1979) Red and photographic infared linear combinations for monitoring vegeation. Remote Sensing of Environment. 8(2), 127-150. https://doi.org/10.1016/0034-4257(79)90013-0

[28] Uelmen, J. A., Mapes, C. D., Prasauskas, A., Boohene, C., Burns, L., Stuck, J., Carney, R. M. (2023) A habitat model for disease vector Ae. aegypti in the Tampa Bay Area, Florida. Journal of the American Mosquito Control Association. 39(2), 96-107. https://doi.org/10.2987/22-7109 Valdez-Delgado, K. M., Garcia-Salazar, O., Moo-Llanes, D.

[29] A., Izcapa-Trevino, C., Cruz-Pliego, M. A., DominguezPosadas, G. Y., Armendariz-Valdez, M. O., Correa-Morales, F., Cisneros-Vazquez, L. A., Ordonez-Gonzalez, J. G., Fernandez-Salas, I., Danis-Lozano, R.

(2023) Mapping the urban environments of Aedes aegypti using drone technology. Drones. 7(9), 581. https://doi.org/10.3390/drones7090581

[30] Simard, F., Nchoutpouen, E., Toto, J.C., Fontenille, D. (2005) Geographic distribution and breeding site preference of Aedes albopictus and Aedes aegypti (Diptera: Culicidae) in Cameroon, Central Africa. Journal of Medical Entomology. 45(5), 726-731. Doi: 10.1093/jmedent/42.5.726.

[31] Tabachnick, W.J. (1991). Evolutionary genetics and arthropod-borne disease: The yellow fever mosquito, American Entomologist. 37(1), 14–26. https://doi.org/10.1093/ae/37.1.14

[32] Wilke, A. B. B., Chase, C., Vasquez, C., Carvajal, A., Medina, J., Petrie, W. D., Beier, J. C. (2019) Urbanization creates diverse aquatic habitats for immature mosquitoes in urban areas. Sciencetific Reports. 9(15335). https://doi.org/10.1038/s41598-019-51787-5

[33] Wikle, C. K., Zammit-Mangion, A., and Cressie, N. (2019), Spatio-Temporal Statistics with R, Boca Raton, FL: Chapman & Hall/CRC. © 2019 Wikle, Zammit-Mangion, Cressie. https://spacetimewithr.org

[34] Zahid, M. H., Van Wyk, H., Morrison, A. C., Coloma, J., Lee, G. O., Cevallos, V., Ponce, P., Eisenberg, J. N. S. (2023) The biting range of Ae. aegypti and its variability: A systematic review (1970-2022). PLOS Neglected Tropical Diseases. https://doi.org/10.1371/journal.pntd.0010831